

Novel high-quality Fano resonance based on metal-insulator-metal waveguide with L-shaped resonators

Changsong Wu(伍长松) and Jun Zhu(朱君)

Citation: Chin. Phys. B, 2021, 30 (**10**): 104210. DOI: 10.1088/1674-1056/abf922
Journal homepage: http://cpb.iphy.ac.cn; http://iopscience.iop.org/cpb

What follows is a list of articles you may be interested in

Controllable four-wave mixing response in a dual-cavity hybrid optomechanical system

Lei Shang(尚蕾), Bin Chen(陈彬), Li-Li Xing(邢丽丽), Jian-Bin Chen(陈建宾), Hai-Bin Xue(薛海斌), and Kang-Xian Guo(郭康贤)
Chin. Phys. B, 2021, 30 (**5**): 054209. DOI: 10.1088/1674-1056/abd695

Dissipative Kerr solitons in optical microresonators with Raman effect and third-order dispersion

Chaohua Wu(吴超华), Zhiwei Fang(方致伟), Jintao Fan(樊景涛), Gang Chen(陈刚), and Ya Cheng(程亚)
Chin. Phys. B, 2021, 30 (**5**): 054206. DOI: 10.1088/1674-1056/abd15f

Generation of wideband tunable femtosecond laser based on nonlinear propagation of power-scaled mode-locked femtosecond laser pulses in photonic crystal fiber

Zhiguo Lv(吕志国) and Hao Teng(滕浩)
Chin. Phys. B, 2021, 30 (**4**): 044209. DOI: 10.1088/1674-1056/abe231

Properties of metal-insulator-metal waveguide loop reflector

Hu Long(龙虎), Xuan-Ke Zeng(曾选科), Yi Cai(蔡懿), Xiao-Wei Lu(陆小微), Hong-Yi Chen(陈红艺), Shi-Xiang Xu(徐世祥), Jing-Zhen Li(李景镇)
Chin. Phys. B, 2019, 28 (**9**): 094215. DOI: 10.1088/1674-1056/ab38a3

Plasmonically induced reflection in metal-insulator-metal waveguides with two silver baffles coupled square ring resonator

Zhi-Dong Zhang(张志东), Lian-Jun Ma(马连俊), Fei Gao(高飞), Yan-Jun Zhang(张彦军), Jun Tang(唐军), Hui-Liang Cao(曹慧亮), Bin-Zhen Zhang(张斌珍), Ji-Cheng Wang(王继成), Shu-Bin Yan(闫树斌), Chen-Yang Xue(薛晨阳)
Chin. Phys. B, 2017, 26 (**12**): 124212. DOI: 10.1088/1674-1056/26/12/124212

Novel high-quality Fano resonance based on metal-insulator-metal waveguide with L-shaped resonators*

Changsong Wu(伍长松) and Jun Zhu(朱君)†

College of Electronic Engineering, Guangxi Normal University, Guilin 541004, *China*

(Received 17 December 2020; revised manuscript received 20 February 2021; accepted manuscript online 19 April 2021)

Developing a convenient method that can be routinely applied for ascertaining proportions of different vegetable oils employed in commercial blended edible oils remains a significant challenge. We address this issue by proposing a novel method for detecting volume fraction of different oils based on the fact that these oils are optically transparent and have slightly different indices of refraction at a given temperature and wavelength. Accordingly, we develop a highly sensitive sensor for measuring the index of refraction of oil blends based on Fano resonance spectra obtained using a metal-insulator-metal (MIM) waveguide structure comprising a gapped straight waveguide coupled with two L-shaped resonators. The index of refraction sensitivity and figure of merit of the structure are calculated based on modeling using the finite element method, and the waveguide structure is accordingly optimized by adjusting the different geometric parameters to achieve a high-quality Fano resonance spectrum. The optimized structure achieves an ultra-high refractive index sensitivity of 770 nm/RIU in terms of a refractive index unit (RIU) of 1. Moreover, a highly stable linear relationship is obtained between the refractive index of mixed edible oils and the resonance wavelength. Experimental results demonstrate that the proposed structure can detect slight changes in the volume fractions of the components in blended oils.

Keywords: Fano resonance refractive index sensing, metal-insulator-metal (MIM) waveguide, volume fraction detection

PACS: 42.65.–k, 42.79.–e, 42.81.Pa, 71.36.+c **DOI:** 10.1088/1674-1056/abf922

1. Introduction

Blended edible oils are prepared using specific proportions of two or more different vegetable oils, such as inexpensive oils like soybean, corn, and rapeseed oils, and relatively expensive oils like sesame seed and peanut oils, which are sold commercially worldwide.[1,2] Blended oils can have many desirable features, including unique aromas and flavors, comprehensive nutrition, and reduced costs.[3] However, manufacturers can engage in unscrupulous activities by adopting an inexpensive vegetable oil as the main component, adding a small amount of relatively expensive vegetable oil, and then marketing the product at a high price as a high-grade vegetable oil.[4,5] While regulatory agencies require that the proportion of vegetable oils be specified on the labels of blended edible oils, the reliability of the reported proportions presently relies only on the self-restraint of the manufacturer and the inspection procedures adopted by the regulatory authority, which remain non-standardized.[6] The most common approach involves detection of molecular components unique to various oils using methods such as high-performance liquid chromatography (HPLC). However, the method is relatively time consuming and requires considerable expertise. Accordingly, developing a convenient, economical, and environmentally friendly method that can be widely and routinely applied for ascertaining proportions of vegetable oils in commercial blended oils stands for a significant challenge.[7]

A particularly convenient approach for determining the proportions of vegetable oils in commercial blended oils could be based on the fact that these oils are optically transparent and have uniform and slightly different indices of refraction at given temperature and wavelength. For example, the refractive indices of peanut oil, soybean oil, and rapeseed oil at room temperature are 1.47161, 1.47510, and 1.47287, respectively.[8] As such, the overall refractive index of a mixture of these three oils will vary according to the mixing ratio by volume. This principle could then be employed for determining the volume fractions of the oils in the blend. However, this approach suffers from the fact that it relies upon extremely small differences in refractive indices, and therefore requires an extremely sensitive approach for measuring the index of refraction of oil blends.[9,10]

This issue can be potentially addressed through the use of surface plasmon polaritons (SPPs), which are longitudinal electromagnetic waves traveling along metal–dielectric interfaces that are generated by the collective oscillation of an incident electromagnetic field and the charge on the metal surface.[11–13] Interestingly, SPPs can overcome the diffraction limit of conventional optical microscopy,[14–16] and have the characteristics of ultra-fast response and ultra-high sensitivity to the index of refraction of the dielectric employed in the metal–dielectric interface.[17–20] In this regard, resonators

*Project supported by the National Natural Science Foundation of China (Grant No. 51965007) and the "One thousand Young and Middle-Aged College and University Backbone Teachers Cultivation Program" of Guangxi, China (Grant No. 2019).

†Corresponding author. E-mail: zhujun1985@gxnu.edu.cn

© 2021 Chinese Physical Society and IOP Publishing Ltd

based on Fano resonance are particularly sensitive to the index of refraction owing to its asymmetrical spectral line shape that causes dramatic intensity changes and wavelength shifts in response to small disturbances in the index of refraction.[21–26] This has led to increasing attention given to SPP devices based on Fano resonance. For example, Zhang *et al.*[27] proposed an index of refraction sensor based on a metal-insulator-metal (MIM) waveguide coupled with two rectangular cavities. The resonator was demonstrated to achieve an index of refraction sensitivity of 596 nm/RIU in terms of a refractive index unit (RIU) of 1. In addition, Chen *et al.*[28] proposed a Fano resonator comprising a single defect nanocavity coupled with a plasmonic waveguide, which achieved a refractive index sensitivity of 700 nm/RIU. However, while these past studies have clearly demonstrated the usefulness of Fano resonators as refractive index sensors, the present state of development offers room for improvement, and the approach has not yet been applied for developing a convenient method for ascertaining the proportions of different vegetable oils employed in commercial blended edible oils.

The present study addresses this issue by proposing a highly sensitive sensor for measuring the index of refraction of oil blends using a MIM waveguide structure comprising a gapped straight waveguide coupled with two L-shaped resonators.[29] The base material of the structure is composed of SiO_2 and the waveguide material is solid metallic elemental silver (Ag), while the boundary conditions are perfectly matched layers (PMLs). The sensor adopts a chemical vapor deposition method to deposit a metal layer on a silicon dioxide base layer. Subsequently, the waveguide and the resonant cavity are etched in the metal layer by an etching method. The index of refraction sensitivity and figure of merit (FOM) of the structure are calculated based on modeling using the finite element method (FEM), and the waveguide structure is accordingly optimized by adjusting the different geometric parameters to achieve a high-quality Fano resonance spectrum. The optimized structure achieves an ultra-high refractive index sensitivity of 770 nm/RIU. Moreover, a highly stable linear relationship is obtained between the refractive index of mixed edible oils and the resonance wavelength. Experimental results demonstrate that the proposed structure can detect slight changes in the volume fractions of the individual components in three-component mixtures of peanut, soybean, and rapeseed oils. This study further provides an important reference supporting the development of similar sensor designs.

2. Structural model and theoretical analysis

2.1. Structural model

The width of the straight waveguide is w, the gap width is d, the two L-shaped resonant cavities have a symmetric structure, each with a height H, length V, and a width along both sides of the L shape that is equivalent to the one of the straight waveguide w, while the interval between the resonant cavities is g and the coupling distance between the resonant cavity and the waveguide is also g. The schematic of the structure is shown in Fig. 1.

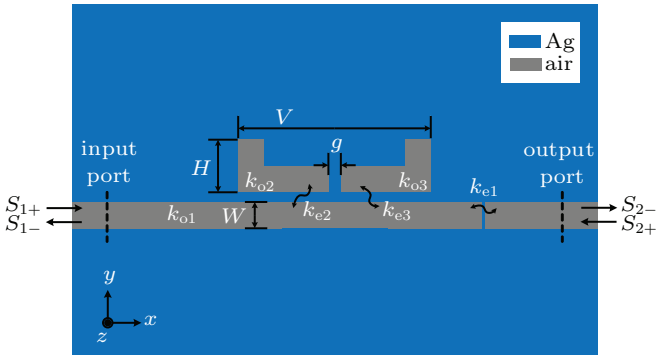


Fig. 1. The proposed Fano resonance structure composed of an MIM waveguide and two coupled L-shaped resonant cavities.

We employ coupled mode theory (CMT) to analyze the Fano resonance produced by the proposed structure.[30] For this purpose, we designate A as the normalized amplitude of the optical transmittance T for the straight waveguide to the left of the gap, and designate B and C as the normalized amplitudes of T for the left and right L-shaped resonators, respectively. The changes in these amplitudes with respect to time t can be expressed as

$$\frac{\mathrm{d}A}{\mathrm{d}t} = (\mathrm{j}\omega_{\mathrm{A}} - k_{\mathrm{o1}}^2 - k_{\mathrm{e1}}^2 - k_{\mathrm{e2}}^2 - k_{\mathrm{e3}}^2)A + k_{\mathrm{e1}}S_{2+} + k_{\mathrm{e2}}B + k_{\mathrm{e3}}C = \mathrm{j}\omega A, \tag{1}$$

$$\frac{\mathrm{d}B}{\mathrm{d}t} = (\mathrm{j}\omega_{\mathrm{B}} - k_{\mathrm{o2}}^2 - k_{\mathrm{e2}}^2)B + k_{\mathrm{e2}}A = \mathrm{j}\omega B, \tag{2}$$

$$\frac{\mathrm{d}C}{\mathrm{d}t} = (\mathrm{j}\omega_{\mathrm{C}} - k_{\mathrm{o3}}^2 - k_{\mathrm{e3}}^2)C + k_{\mathrm{e3}}A = \mathrm{j}\omega C. \tag{3}$$

Here, ω_{A}, ω_{B}, and ω_{C} are the respective resonant frequencies of the straight waveguide to the left of the gap and the left and right L-type resonators k_{o1}, k_{o2}, k_{o3}, and are the internal attenuation loss coefficients, k_{e1} is the coupling coefficient of the left and right sections of the straight waveguide, k_{e2} and k_{e3} are the respective coupling coefficients of the straight waveguide to the left of the gap and the left and right L-shaped resonators, S_{1+} and S_{2+} represent the mode field amplitudes of incident light at the port, S_{1-} and S_{2-} represent the mode field amplitudes of outgoing light. Finally, Eqs. (1)–(3) are combined to obtain the transmittance T of the proposed structure as follows:

$$T = k_{\mathrm{e1}}\left|\left[\mathrm{j}(\omega-\omega_{\mathrm{A}}) + k_{\mathrm{o1}}^2 + k_{\mathrm{e1}}^2 + k_{\mathrm{e2}}^2 + k_{\mathrm{e3}}^2\right] - \frac{k_{\mathrm{e2}}^2}{\mathrm{j}(\omega-\omega_{\mathrm{B}}) + k_{\mathrm{o2}}^2 + k_{\mathrm{e2}}^2} - \frac{k_{\mathrm{e3}}^2}{\mathrm{j}(\omega-\omega_{\mathrm{C}}) + k_{\mathrm{o3}}^2 + k_{\mathrm{e3}}^2}\right|^{-2}. \tag{4}$$

In transverse magnetic (TM) mode, the dispersion relation of SPPs in an MIM waveguide structure is given as

follows:[31,32]

$$\tanh\left(\frac{\mathrm{d}\sqrt{\beta^2-k_0^2\varepsilon_{\mathrm{in}}}}{2}\right)=\frac{-\varepsilon_{\mathrm{in}}\sqrt{\beta^2-k_0^2\varepsilon_{\mathrm{in}}\varepsilon_{\mathrm{m}}(\omega)}}{\varepsilon_{\mathrm{m}}(\omega)\sqrt{\beta^2-k_0^2\varepsilon_{\mathrm{in}}}}. \quad (5)$$

Here, the wave vector in free space is denoted as $k_0=2\pi/\lambda$, where λ is the wavelength of the incident light, the propagation constant is denoted as $\beta=n_{\mathrm{eff}}\times k_0$, with n_{eff} being the effective refractive index of the waveguide structure, $\varepsilon_{\mathrm{in}}$ the dielectric constant of the insulator medium, and $\varepsilon_{\mathrm{m}}(\omega)$ the dielectric constant of the metal, which is a function of the angular frequency ω of the incident light. The optical frequency characteristics of metals can be illustrated by ignoring the interactions of free electrons and electrons or ions in the metal, which enables the application of the following Drude model:[33–36]

$$\varepsilon_{\mathrm{m}}(\omega)=\varepsilon_{\infty}-\frac{\omega_{\mathrm{p}}^2}{\omega^2-\mathrm{i}\omega\gamma}, \quad (6)$$

where $\varepsilon_{\infty}=3.7$ is the dielectric constant of the metal at ω approaching infinity, $\omega_{\mathrm{p}}=9.1$ Hz is the plasma oscillation frequency, and $\gamma=0.018$ Hz is the electron collision frequency.

In this study, we define the sensitivity of the sensor as the shift in the resonance wavelength $\Delta\lambda$ of the waveguide with respect to changes in the refractive index Δn, which is formally given as $S=\Delta\lambda/\Delta n$ (nm/RIU).[37] In addition, the FOM is adopted as another important indicator to evaluate sensor performance.[38,39] Here, the FOM is a dimensionless parameter that reflects the relationship between S and the sensor resolution, and is given as FOM $=S/$FWHM, where FWHM is the full width at half maximum of the Fano resonance peak, which decreases with increasing sensor resolution.[40] Accordingly, the FOM increases when S increases and/or when the FWHM decreases, which is indicative of increasing sensor performance.

2.2. Theoretical analysis

The theoretical transmittance spectra of the proposed MIM waveguide structure are presented in Fig. 2. Here, Fig. 2(a) presents the transmittance spectrum of the gapped waveguide alone, Fig. 2(b) presents the transmittance spectrum of the coupled straight waveguide and L-shaped resonant cavities alone, and Fig. 2(c) presents the transmittance spectrum of the coupled gapped waveguide and resonant cavity system. The results demonstrate that the gapped waveguide alone generates a wide and nearly continuous transmittance spectrum, which is generated under the excitation of the incident light and the SPPs it produces. Accordingly, this can be viewed as a broad continuous state.[41,42] In contrast, the L-shaped resonant cavities alone exhibit a very narrow stop band centered at a wavelength of 813 nm, which can be viewed as a narrow discrete state.[43] Finally, the coupled waveguide and resonant cavity system generates a Fano resonance spectrum with an asymmetrical sharp peak labeled as Peak, a major trough labeled as dip I, and a minor trough labeled as dip Ⅱ, which are formed by the coherent superposition of the straight waveguide and resonant cavities in accordance with the respective transmittance spectra in Figs. 2(a) and 2(b).[44]

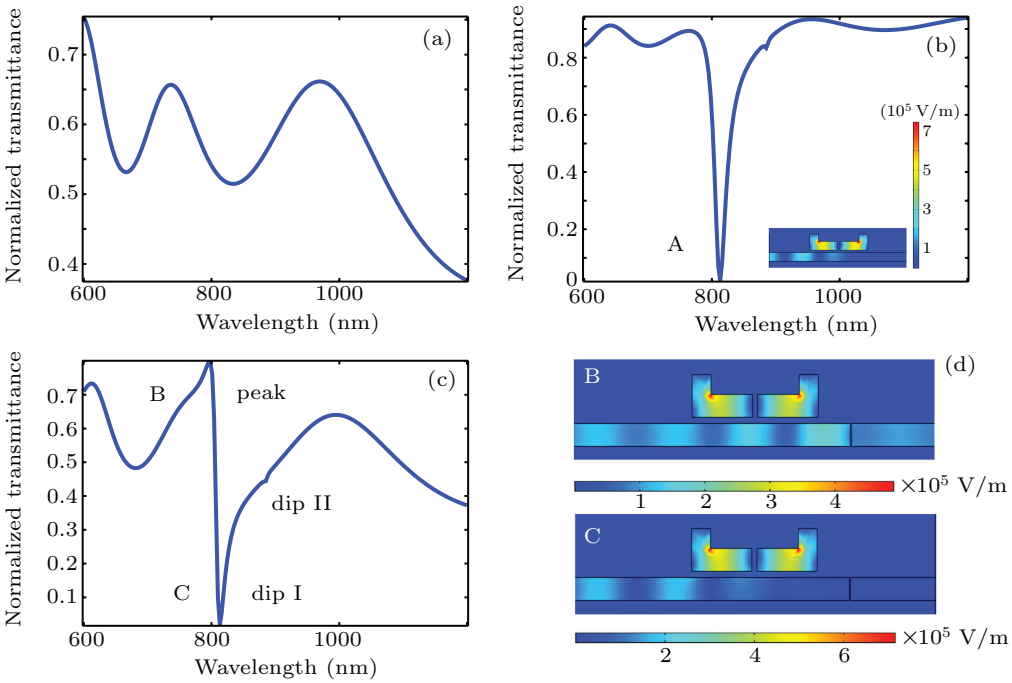


Fig. 2. Transmittance spectra of the proposed Fano resonance structure composed of an MIM waveguide and two coupled L-shaped resonant cavities: (a) gapped waveguide only; (b) L-shaped resonant cavities only; (c) coupled gapped waveguide and resonant cavity system. (d) Electric field intensity distribution diagrams at the two points B, and C.

Additionally, in order to analyze the formation mechanism of Fano resonance, the present experiment used the finite element method to calculate the electric field intensity distribution at the three points marked by A, B and C in Fig. 2. It can be seen from the electric field intensity of A in Fig. 2(b) that the electric field intensity on the right side of the straight waveguide is significantly smaller than the electric field intensity on the left side. The coupling between the straight waveguide and the two L-shaped resonators causes most of the energy to be concentrated on the left side of the straight waveguide. Furthermore, the transmission spectrum forms a narrow discrete state at the wavelength of 813 nm. After adding a gap on the right side of the waveguide, SPPs propagating are blocked back. Some SPPs near-field coupling leads to interference can be canceled and the other part is coupled with the L-shaped cavity. This can be clearly seen from Fig. 2(d) (top). The electric field intensity is quite uniform on both sides of the gap waveguide, which leads to the high transmittance shown in Fig. 2(c).[45] Continue to increase the electric field intensity, the more the electric field bounces back by the gap and the stronger the interference cancelation is. Finally, the critical state is reached at the wavelength of 813 nm. As shown in in Fig. 2(d) (bottom), almost no electric field passes through the right side of the main waveguide. A great quantity of electric fields is coupled in the L-type resonator. The maximum electric field intensity difference between the two points B and C is 260 V/m at 798 nm. The electric field intensity distribution diagrams at points A, B, and C clearly illustrate the formation process of a Fano resonance spectrum.

3. Structural parameter analysis

The structural design of the proposed resonator is optimized in this section in terms of the FWHM values of the Peak and dip I features of the Fano resonance spectrum obtained by the resonator during variations in the values of the structural parameters H, V, w, and g individually, while holding all other parameters constant. The width d value is fixed at 5 nm to ensure that the gap in the straight waveguide remains narrow. Unless otherwise specified, the standard parameters employed were $H = 135$ nm, $V = 500$ nm, $w = 75$ nm, $g = 20$ nm, and $d = 5$ nm, and these standard values were replaced with the optimal values obtained after each of the individual optimization processes. In addition, the refractive index n of the dielectric was assumed to be 1 throughout all optimization processes. We can obtain the normalized transmittance of the proposed structure in conjunction with Eq. (4).

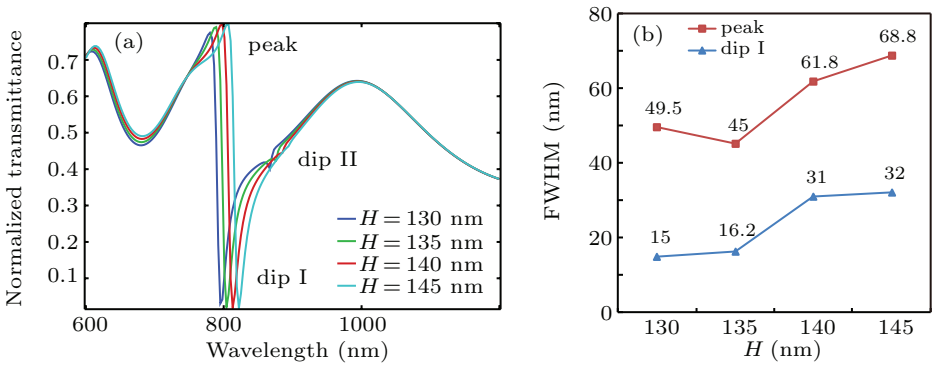


Fig. 3. Optimization of the proposed Fano resonance structure with respect to the height H of the L-shaped resonant cavities varied from 130 nm to 145 nm: (a) transmittance spectra, (b) full width at half maximum (FWHM) of the Fano resonance features peak and dip I.

The transmittance spectra obtained by the proposed resonator for different values of H in the range of 130 nm to 145 nm are presented in Fig. 3(a), while the FWHM of the peak and dip I features of the Fano resonance spectrum are presented in Fig. 3(b). This range of H was selected because insufficient coupling was obtained between the straight waveguide and the resonant cavities for values lying outside of this range, resulting in flat transmittance spectra. We note from Fig. 3(a) that the central wavelength λ_{Peak} of the peak feature shifts to longer wavelengths from 780 nm to 804 nm with increasing H, while the corresponding transmittance increases from 0.774 to 0.797. Similarly, the central wavelength $\lambda_{\text{Dip I}}$ of the dip I feature shifts from 795 nm to 822 nm and the corresponding transmittance decreases from 0.031 to 0.019. We also note from Fig. 3(b) that the FWHM values of peak are always greater than those of dip I, and both values generally increase with increasing H from 130 nm to 145 nm. The only exception is observed for the FWHM of peak at $H = 135$ nm, which presents a minimum value. These results indicate that 135 nm is the optimal value of H because the difference between the FWHM values of peak and dip I is smallest at this point, and both features have relatively low FWHM values.

The transmittance spectra obtained by the proposed resonator for different values of V in the range of 470 nm to 500 nm are presented in Fig. 4(a), while the FWHM of the peak and dip I spectral features are presented in Fig. 4(b). This range of V was selected because insufficient coupling was obtained between the straight waveguide and the resonant cavi-

ties for values lying outside of this range, resulting in flat transmittance spectra. We note from Fig. 4(a) that λ_{Peak} shifts from 747 nm to 789 nm with increasing V, while the corresponding transmittance increases from 0.62 to 0.79. Similarly, $\lambda_{\text{Dip I}}$ shifts from 765 nm to 804 nm, and the corresponding transmittance decreases from 0.06 to 0.02. We also note from Fig. 4(b) that the FWHM values of peak are always greater than those of dip I, and both values increase monotonically with increasing V from 470 nm to 500 nm. These results indicate that 470 nm is the optimal value of V because the difference between the FWHM values of peak and dip I is smallest at this point, and both features have their lowest FWHM values. This was employed as the standard value of V in all subsequent optimization processes.

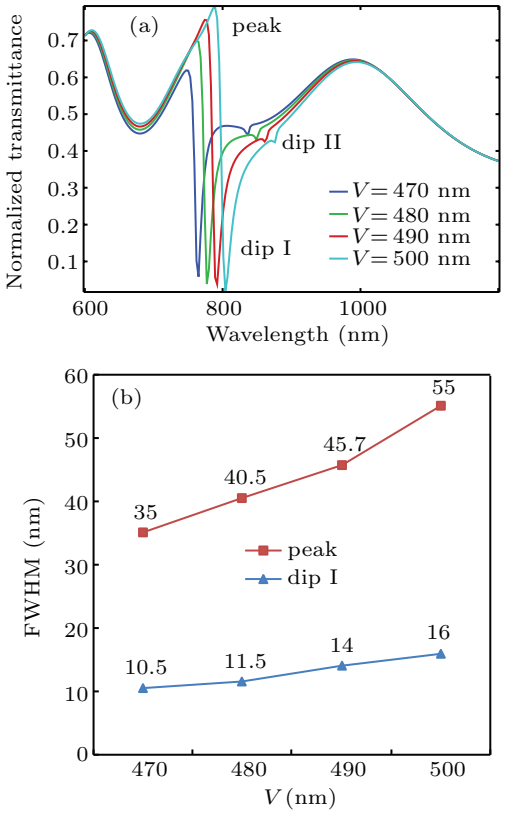


Fig. 4. Optimization of the proposed Fano resonance structure with respect to the length V of the L-shaped resonant cavities varied from 470 nm to 500 nm: (a) transmittance spectra, (b) FWHM of peak and dip I spectral features.

The transmittance spectra obtained by the proposed resonator for different values of w in the range of 74 nm to 80 nm are presented in Fig. 5(a), while the FWHM of peak and dip I are presented in Fig. 5(b). This range of w was selected because insufficient coupling was obtained between the straight waveguide and the resonant cavities for values lying outside of this range, resulting in flat transmittance spectra. We note from Fig. 5(a) that λ_{Peak} shifts to shorter wavelengths from 768 nm to 738 nm with increasing w, and the corresponding transmittance decreases from 0.715 to 0.625. Similarly, $\lambda_{\text{Dip I}}$ also shifts to shorter wavelengths from 783 nm to 756 nm. Here, the transmittance first increases from 0.036 to 0.045 with increasing w from 74 nm to 78 nm, and then decreases at $w = 80$ nm. We also note from Fig. 5(b) that the FWHM values of peak are always greater than those of dip I, and both values decrease with increasing w from 74 nm to 80 nm. These results indicate that 80 nm is the optimal value of w because the difference between the FWHM values of peak and dip I is smallest at this point, and both features have their lowest FWHM values. This was employed as the standard value of w in the following optimization process.

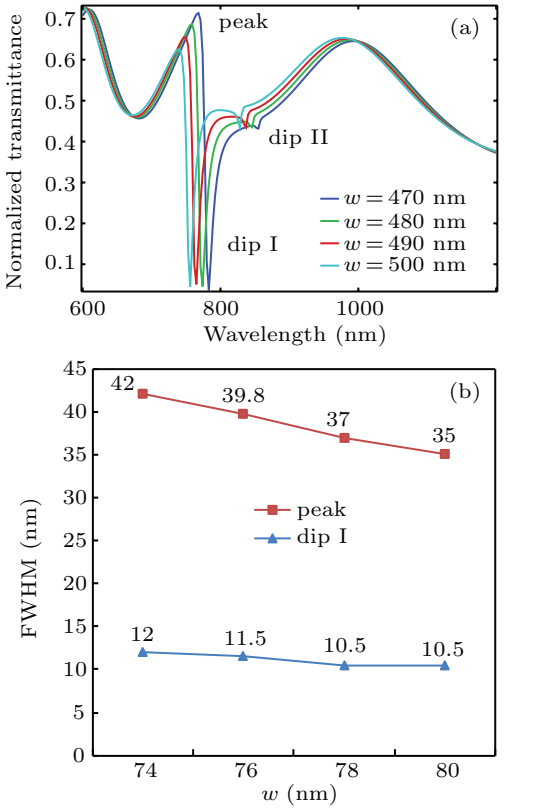


Fig. 5. Optimization of the proposed Fano resonance structure with respect to the width w of the straight waveguide and L-shaped resonant cavities varied from 74 nm to 80 nm: (a) transmittance spectra, (b) FWHM of peak and dip I spectral features.

Finally, the transmittance spectra obtained by the proposed resonator for different values of g in the range from 16 nm to 22 nm are presented in Fig. 6(a), while the FWHM of peak and dip I are presented in Fig. 6(b). We note from Fig. 6(a) that λ_{Peak} shifts to shorter wavelengths from 747 nm to 735 nm with increasing g, and the corresponding transmittance increases from 0.589 to 0.634. Similarly, $\lambda_{\text{Dip I}}$ also shifts to shorter wavelengths, and the transmittance also increases with increasing g. We further note that dip Ⅱ becomes quite prominent at relatively small values of g, and presents a very similar behavior to that of dip I. With respect to the FWHM, we again note from Fig. 6(b) that the FWHM values of peak are always greater than those of dip I, and both values decrease monotonically with increasing g. This decrease in the FWHM values is particularly prominent for dip I, where

the FWHM obtained at $g = 16$ nm is nearly twice that obtained at $g = 22$ nm. Therefore, 22 nm was selected as the optimal value of g.

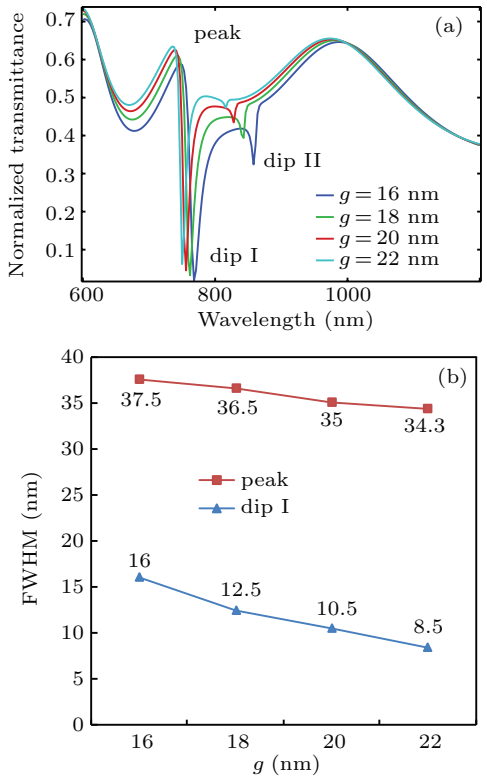


Fig. 6. Optimization of the proposed Fano resonance structure with respect to the gap distance g between the straight waveguide and L-shaped resonant cavities and between the two L-shaped resonant cavities varied from 16 nm to 22 nm: (a) transmittance spectra, (b) FWHM of peak and dip I spectral features.

4. Refractive index sensitivity and application to mixed oil analysis

4.1. Sensitivity analysis

The optimized structural design of the proposed resonator with $H = 135$ nm, $V = 470$ nm, $w = 80$ nm, $g = 224$ nm, and $d = 5$ nm was applied to evaluate its sensitivity to the refractive index n of the dielectric based on a control variable method to that applied in Sections 2 and 3. The transmittance spectra obtained for n varied over the narrow range of 1.0 to 1.08 are presented in Fig. 7(a), while λ_{Peak}, $\lambda_{\text{Dip I}}$, and the central wavelength $\lambda_{\text{Dip II}}$ of the dip II feature of the Fano resonance spectra are presented in Fig. 7(b) as a function of n.

Here, dip II is used to assist in the detection process, as discussed elsewhere.[46] We note from Fig. 7(a) that λ_{Peak} shifts by 57 nm to higher wavelengths from 735 nm to 792 nm with increasing n from 1.0 to 1.08. Similarly, $\lambda_{\text{Dip I}}$ shifts by 57 nm from 750 nm to 807 nm, and $\lambda_{\text{Dip II}}$ shifts by 62 nm from 816 nm to 878 nm. We also note that λ_{Peak}, $\lambda_{\text{Dip I}}$, and $\lambda_{\text{Dip II}}$ all vary linearly with respect to n, and that the refractive index sensitivity S of each resonance feature is the slope of the corresponding line (i.e., $\Delta\lambda/\Delta n$). Accordingly, the values of S can be obtained by applying linear fitting to the λ versus n plots in Fig. 7(b), which yield S values of 705 nm/RIU, 720 nm/RIU, and 770 nm/RIU for peak, dip I, and dip II, respectively. Moreover, the results of fitting to the λ_{Peak}, $\lambda_{\text{Dip I}}$, and $\lambda_{\text{Dip II}}$ values yield coefficient of determination R^2 values of 0.9986, 0.9983, and 0.9915, respectively. These represent nearly perfect linear relationships, which demonstrate that the value of an unknown n can be obtained from a suitably calibrated linear plot of known values of n. In addition, we obtain the FWHM values of 34.3 nm, 8.5 nm, and 5 nm for peak, dip I, and dip II, respectively. Therefore, the calculated FOM values for peak, dip I, and dip II are 20.56, 84.7, and 154, respectively. Accordingly, we can conclude that dip II provides the highest S and FOM values of all Fano resonance spectrum features considered. In addition, the obtained value of S is compared with those obtained in other studies applying Fano resonance in Table 1, where we note that the presently proposed approach achieves a value that is between 2.5% and 29.2% greater than these previous results.

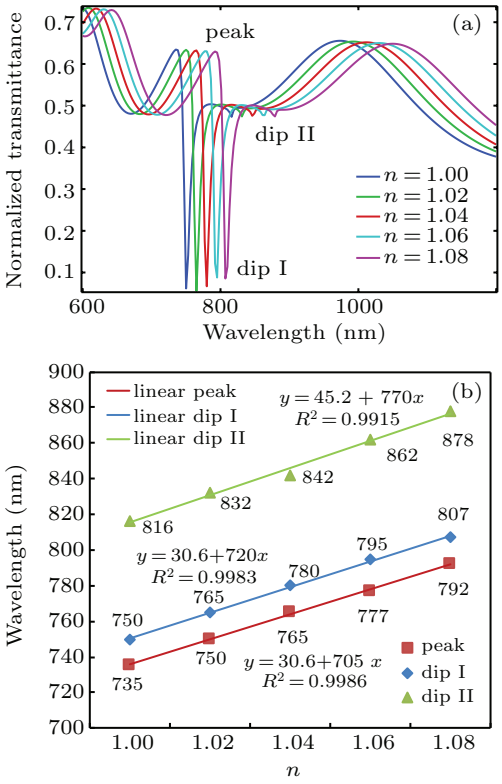


Fig. 7. (a) Transmittance spectra of the optimized Fano resonance structure for different values of the refractive index n of the dielectric ranging from 1.0 to 1.08. (b) Central wavelengths of the Fano resonance features in (a) with respect to n.

Table 1. Refractive index sensitivity values reported for various studies employing Fano resonance.

Source	Sensitivity (nm/RIU)
Zhang *et al.*[27]	596
He *et al.*[46]	626
Caballero *et al.*[47]	659
Chen *et al.*[29]	700
Chen *et al.*[30]	750
This paper	770

4.2. Mixed oil analysis

The proposed resonator design was applied to blends of peanut oil, rapeseed oil, and soybean oil, which used the known refractive index value of the mixture to replace the actual mixture for subsequent experiments. The refractive index Y for blends of peanut oil (X_1, $n = 1.47161$), soybean oil (X_2, $n = 1.47510$), and rapeseed oil ($n = 1.47287$) is given as follows:[8]

$$Y = 1.472679143 - 0.0008354285714X_1 + 0.0025622857143X_2, \quad (7)$$

where the constant volume fraction $X_2 = 10\%$ of soybean oil and the volume fractions X_1 are set as the dependent variables, and any remaining volume fraction is for rapeseed oil. The volume fraction of rapeseed oil is ignored because it has no considerable effect on the value of Y.[8] We note from Eq. (7) that Y will vary linearly with respect to X_1 if the value of X_2 is a constant. Accordingly, we can expect from the linearity of λ_{Peak}, $\lambda_{\text{Dip I}}$, and $\lambda_{\text{Dip II}}$ with respect to n discussed in Subsection 4.1 that the λ_{Peak}, $\lambda_{\text{Dip I}}$, and $\lambda_{\text{Dip II}}$ values of these blends would vary linearly with respect to changes in X_1, while holding X_2 constant. Therefore, the value of X_2 was set to 10% in all experiments, and the value of X_1 was varied in the range of 0%–90% in intervals of 10%, while rapeseed oil was applied for any remaining volume fraction. The transmittance spectra obtained with the different values of X_1 are presented in Fig. 8. We note that the overall Fano resonance spectrum shifts in miniscale increments toward higher wavelengths with increasing X_1, which is more clearly indicated by the shift in dip I shown in the inset of the figure.

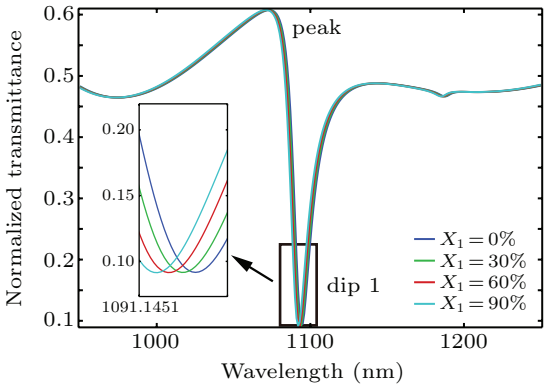


Fig. 8. CMT principle based experimental transmittance spectra from CMT principle of the proposed Fano resonance structure for blended peanut, soybean, and rapeseed oils with different known refractive index.

The values of Y calculated from Eq. (7) and the values of λ_{Peak}, $\lambda_{\text{Dip I}}$, and $\lambda_{\text{Dip II}}$ obtained from the transmittance spectra of all oil mixtures considered are listed in Table 2. The data derived from Table 2 is plotted in Fig. 9 along with the results of linear fitting. The fitted results yield the linear equations $\lambda_{\text{Peak}} = 1073.3945–2.4545X_1$, $\lambda_{\text{Dip I}} = 1094.5036–2.6303X_1$ with R^2 values of 0.9844, 0.9848, respectively, over a range of Y from 1.4719 to 1.4750. Again, the goodness of fit represents nearly perfect linear relationships, indicating that the volume fraction of peanut oil can be determined for such three-component mixture containing soybean oil, peanut oil and rapeseed oil. An analysis of the sensitivity of $\lambda_{\text{Dip I}}$ to changes in Y along with the corresponding FWHM values of the dip I features indicates that a maximum FOM value of 1666.6 is obtained at $X_1 = 50\%$.

Table 2. Refractive index Y of blended peanut, soybean, and rapeseed oils based on Eq. (7) and the central wavelengths of the Fano resonance features denoted as peak and dip I with different volume fractions X_1 of peanut oil, where the volume fraction of soybean oil is fixed at 10%, and rapeseed oil was applied to any remaining volume fraction.

X_1	Y	λ_{Peak}	$\lambda_{\text{Dip I}}$
0%	1.4750	1073.5	1094.5
10%	1.4746	1073.1	1094.1
20%	1.4743	1073.0	1094.0
30%	1.4740	1072.6	1093.7
40%	1.4736	1072.2	1093.7
50%	1.4733	1072.2	1093.2
60%	1.4729	1071.9	1092.9
70%	1.4726	1071.7	1092.6
80%	1.4723	1071.7	1092.4
90%	1.4719	1071.2	1092.1

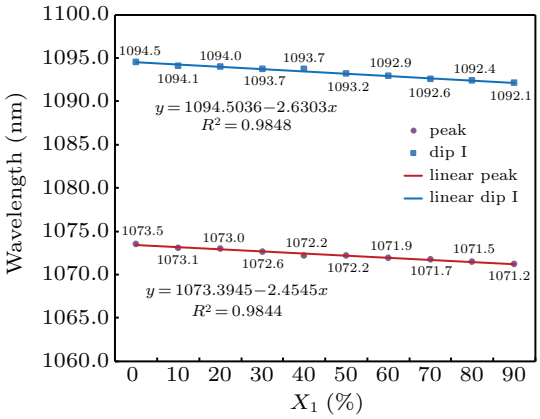


Fig. 9. Plots of the central wavelengths of the Fano resonance features denoted as peak and dip I listed in Table 2 for blended peanut, soybean, and rapeseed oils with respect to volume fraction X_1, along with the results of linear fitting to the data.

5. Conclusion

The present work has addressed the significant challenge associated with developing a convenient method that can be routinely applied for ascertaining the proportions of different vegetable oils employed in commercial blended edible oils by proposing a highly sensitive sensor for measuring the index of refraction of oil blends based on Fano resonance spectra obtained using an MIM waveguide structure comprising a gapped straight waveguide coupled with two L-shaped resonators. The index of refraction sensitivity and FOM of the structure are calculated based on modeling using the FEM, and the waveguide structure is accordingly optimized by adjusting the different geometric parameters to achieve a high-quality

Fano resonance spectrum. The optimized structure achieved an ultra-high refractive index sensitivity of 770 nm/RIU with respect to the dip Ⅱ feature of the Fano resonance spectrum. Moreover, a highly stable linear relationship is obtained between the refractive index of the dielectric and the resonance wavelength of all three spectral features. Experimental applications of the proposed resonance structure to different mixtures of peanut, soybean, and rapeseed oils yield linear representations of the central wavelengths of the spectral features with respect to variations in the volume fraction of peanut oil in the mixture while the volume fraction of soybean oil is held constant. Accordingly, the volume fraction of peanut oil can be determined for any such three-component mixture that has a known volume fraction of soybean oil. This study further provides an important reference supporting the development of similar sensor designs.

References

[1] Ghosh M, Begg F and Bhattacharyya D T 2017 *J. Oleo Sci.* **66** 217
[2] Xiang W and Gong Q 2020 *J. Sci. Food Agr.* **100** 1124
[3] Xu J, Wang Y T and Liu X F 2015 *Opt. Spectrosc.* **118** 663
[4] Gong W, Shi R and Chen M 2019 *J. Food Meas. Charact.* **13** 2203
[5] Wang X G and Jin Q Z 2018 *Chin. Oils Fats* **43** 1 (in Chinese)
[6] Yang H, Tong P J and Jiang Y R 2017 *J. Am. Oil Chem. Soc.* **94** 631
[7] He D P, Luo Z and Gao P 2020 *Sci. Tech. Cereals, Oils Foods* **28** 1
[8] Xin L and Shi J 2012 *Sci. Technol. Food Ind.* **33** 317 (in Chinese)
[9] Wang L 2010 *Research on the Quality and Safety of Edible Blended Vegetable Oil and Supervision Program* (PhD Dissertation) (Hunan: Hunan Agricultural University) (in Chinese)
[10] Zhang J H, Bian J M and Liu W 2017 *Hunan Agr. Sci.* **3** 109
[11] Zhu J and Li N 2020 *Opt. Express* **28** 19978
[12] Zhu J and Xu Z J 2019 *Opt. Mater. Express* **9** 435
[13] Xu J, Wang Y T and Liu X F 2015 *Opt. Spectrosc.* **118** 663
[14] Akram H and Pierre B 2017 *Opt. Express* **25** 18566
[15] Gao L, Gao W Z and Luo Z C 2019 *Infr. Laser Eng.* **48** 163
[16] Zhu J, Qin L L and Song S X 2016 *Infr. Laser Eng.* **45** 158
[17] Zhu J and Lou J 2020 *Results Phys.* **18** 103183
[18] Zhu J, Xu Z J, Cong H, Fu D L and Wei D Q 2019 *Measurement* **144** 67
[19] Zhu Q Y, Loke S W, Rolando T R, Frank J and Yong X 2019 *ACM Comput. Technol. J.* **52** 1
[20] Jiang F, Dong D, Cao L and Frater M R 2013 *IEEE Trans. Netw. Serv.* **10** 255
[21] Jiang F, Xia H, Tran Q A, Ha Q M, Tran N Q and Hu J 2017 *Knowl.-Based Syst.* **130** 90
[22] Ni B, Chen X Y, Xiong D Y, Liu H, Hua G H and Chang J H 2015 *Opt. Quantum Electron.* **47** 1339
[23] Chen Z and Yu L 2014 *IEEE Photon. J.* **6** 1
[24] Li C, Li S L and Wang Y L 2017 *IEEE Photon. J.* **9** 1
[25] Luk'Yanchuk B, Zheludev N I, Maier S A, Halas N J, Nordlander P and Giessen H 2010 *Nat. Mater.* **9** 707
[26] Wang J, Wang Y, Zhang X, Yang K, Wang Y and Liu S 2011 *Optik* **122** 1808
[27] Zhang Z D, Luo L, Xue C Y, Zhang W D and Yan S B 2016 *Sensors* **16** 642
[28] Chen J, Sun C and Gong Q 2014 *Opt. Lett.* **39** 52
[29] Kim K Y, Cho Y K, Tae H S and Lee J H 2006 *Opt. Express* **14** 320
[30] Chen H B, Zhang Z D, Yan S B and Jiao G T 2016 *Acta Photon. Sin.* **45** 0823002 (in Chinese)
[31] Zhu J, Xu W J, Xu Z J, Fu D L, Song S X and Wei D Q 2017 *Optik* **134** 187
[32] Ni G X, Mcleod A S, Sun Z, Wang L, Xiong L and Post K W 2018 *Nature* **557** 530
[33] Watanabe Y, Hino K I, Hase M and Maeshima N 2017 *Phy. Rev. B* **95** 014301
[34] Wen K, Hu Y, Chen L, Zhou J, Lei L and Meng Z 2016 *Plasmonics* **11** 315
[35] Yu S L, Zhao T G, Yu J G and Pan D F 2019 *Sensors* **19** 1559
[36] Chen L, Liu Y, Yu Z, Wu D, Ma R and Zhang Y 2016 *Opt. Express* **24** 9975
[37] Wang S, Yu S, Zhao T, Wang Y and Shi X 2020 *Opt. Commun.* **465** 125614
[38] M A Butt, N L Kazanskiy and S N Khonina 2020 *Laser Phys.* **30** 076204
[39] Li Z F, Wen K H, Lei L, Zhou J Y, Zhou D Y, Fang Y H and Wu B Y 2019 *IEEE Access* **7** 59369
[40] Zhang Z D, Wang H Y and Zhang Z Y 2013 *Plasmonics* **8** 797
[41] Zhang Y, Li S, Chen Z, Jiang P, Jiao R, Zhang Y, Wang L and Yu L 2016 *Plasmonics* **12** 1099
[42] Zhang Z D, Ma L J, Gao F, Zhang Y J, Tang J and Cao H L 2017 *Chin. Phys. B* **26** 124212
[43] Chen J, Xu R, Mao P, Zhang Y, Liu Y and Tang C 2015 *Plasmonics* **10** 341
[44] Zhou H, Gao D and Gao L 2018 *Plasmonics* **13** 623
[45] Chen S, Meng L, Hu J and Yang Z 2015 *Plasmonics* **10** 71
[46] He J, Fan C, Wang J, Ding P, Cai G and Cheng Y 2013 *J. Opt.* **15** 025007
[47] Caballero B, García-Martín A and Cuevas J C 2016 *ACS Photon.* **3** 203